Time-of-Flight Mobilities for Conducting Dendrimers Composed of *p*-Phenylenevinylene Dendron and Triphenylamine Surface Group

Masanobu Mizusaki

Corporate Research and Development Group, Sharp Corp., 2613-1 Ichinomoto-cho, Tenri, Nara 632-8567, Japan

Received 6 March 2011; accepted 16 May 2011
DOI 10.1002/app.34925
Published online 2 September 2011 in Wiley Online Library (wileyonlinelibrary.com).

ABSTRACT: Charge-carrier transport property of the conducting dendrimer films composed of *p*-phenylenevinylene with generation numbers of two and three as a dendron and triphenylamine as a surface group, which were prepared by spin-coating from the chloroform solutions, was investigated by a time-of-flight technique. For both dendrimer films, hole-carrier transport took place preferentially compared with electron-carrier transport, and typical dispersive hole-carrier transport was observed. The hole-carrier drift mobilities of the two-generation dendrimer film were one order of magnitude larger than those of the three-generation dendrimer film. The difference of the hole-carrier drift mobilities between the two-generation and three-generation dendrimers was due to the difference of the molecular geometric structure and/or the difference of the molecular weight ratio of nitrogen atom in the triphenylamine unit to the dendrimer molecule. © 2011 Wiley Periodicals, Inc. J Appl Polym Sci 123: 3090–3097, 2012

Key words: soluble conducting dendrimers; generation; time-of-flight technique; drift mobility

INTRODUCTION

Electronic and optoelectronic devices using organic materials as active elements, for instance, organic light-emitting diodes (OLEDs), organic field-effect transistors (OFETs), organic photovoltaic cells (OPVs), and so forth, have recently received a great deal of attention from the standpoint of potential technological applications as well as fundamental science.[1–5] Those devices using organic materials have attracted considerable interest because the devices exhibit potentially unique features such as light weight and flexibility.[6–10] Hence the OLEDs have already found practical applications in small sized displays such as mobile phones, digital camera finders, and car audios.[11] However, they are still under development for large-sized flat panel displays and lightings. To achieve the above goal, it is significantly important to form uniform and smooth thin films without roughness and pinholes. Shirota and coworkers[12–17] have proven that amorphous molecular materials are excellent materials for use in OLEDs because they form uniform and smooth thin films without pinholes. As the amorphous molecular materials, star-shaped compounds have been developed such as families of 4,4′,4″-tris(diphenylamino)-triphenylamine,[12–14] 1,3,5-tris(diphenylamino)benzene,[15,16] and 1,3,5-tris[4-(diphenylamino)phenyl]-benzene.[17] These star-shaped compounds are particularly useful for charge-carrier transport and emission materials for OLEDs.

Another advantage of the amorphous molecular materials is that the isotropic optical and charge-carrier transport properties are obtained.[18–20] Organic materials based on π-conjugated systems such as oligothiophenes are known to show highly anisotropic electronic properties.[5,21,22] This point has been clearly demonstrated on OFETs based on thin films of oligothiophenes for which their high hole-carrier mobility is obtained when the oligothiophene molecules are oriented perpendicularly to the substrate.[5,21,22] However, such an orientation is detrimental for OLEDs because it strongly reduces the efficiency of charge-carrier transport through the film thickness.[18–20] To solve this problem, the use of amorphous molecular materials with three-dimensional π-conjugated molecules is suggested by Shirota and coworkers[11–17] and Roncali and coworkers.[18–20] The materials they previously prepared exhibited mostly nondispersive photocurrent decay, and their hole-carrier drift mobilities varied from 10^{-6} to 10^{-2} [$cm^2/(V \cdot s)$] by a time-of-flight (TOF) technique.[11] However, the thin films with those amorphous molecular materials have been prepared by sublimation in vacuum deposition systems.

On the contrary, it is well-known that π-conjugated polymer materials such as poly(3-alkylthiophene)s,[6,23] poly(*p*-phenylenevinylene)s,[24–26] and so

Correspondence to: M. Mizusaki (mizusaki.masanobu@sharp.co.jp).

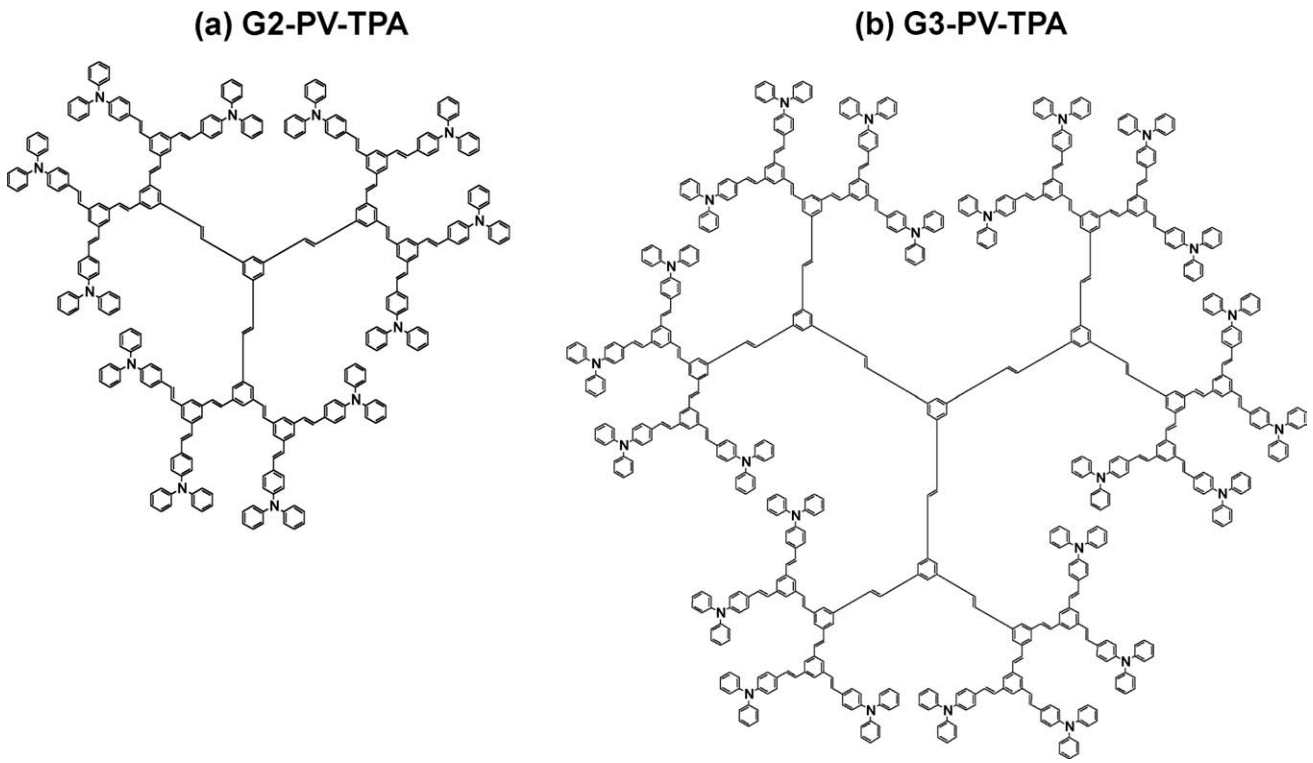

Figure 1 Chemical structures of (a) two-generation dendrimer (G2-PV-TPA) and (b) three-generation dendrimer (G3-PV-TPA) used in this study.

forth can prepare the thin films from the solutions with spin-coating, casting, dipping, and ink-jet techniques without the vacuum system. This is significantly important because the thin films can be prepared with large area easily. However, these π-conjugated polymers are not the three-dimensional materials. Thus, we decided to focus on dendrimer,[27,28] which consists of a core, branching unit termed dendron, and surface group as the three-dimensional macromolecular materials.

In this study, we attempted to characterize the charge-carrier transport property of the dendrimer films composed of *p*-phenylenevinylene dendron with two and three generations and triphenylamine surface group (Fig. 1) by using the TOF technique. The TOF technique is a useful tool to evaluate the charge-carrier transport property through the film thickness. For TOF characterization, sandwich cells of ITO/dendrimer/Mg–Al were prepared, where the dendrimer films were formed from the chloroform solution.

EXPERIMENTAL

Materials

The chemical structures of the two- and three-generation dendrimers, G2-PV-TPA and G3-PV-TPA, are shown in Figure 1(a,b), respectively. The dendrons are constructed from *p*-phenylenevinylene, and the surface groups are from triphenylamine. The synthesized procedure was reported previously.[29] The calculated molecular weights, the weight and number average molecular weights and the polydispersity indices are listed in Table I. The weight and number average molecular weights and the polydispersity indices are estimated by gel permeation chromatography (GPC) with use of THF as eluent and polystyrene standards for calibration. The dendrimers are estimated to be mixtures of *trans*- and *cis*-conformations. Those dissolve in chloroform up to concentrations of 15 mg/mL.

Preparation of cells

The cells of indium-tin-oxide (ITO), dendrimers, and alloy of Mg and Al (Mg–Al), ITO/(G2-PV-TPA or G3-PV-TPA)/Mg–Al, were prepared as follows: First, solutions of the dendrimers were prepared in chloroform at concentrations of 10 mg/mL. The ITO substrates were masked, patterned, and cleaned by sonication in 0.2*M* aqueous NaOH and deionized water. Dendrimer films were prepared from the chloroform solutions onto the cleaned ITO substrates by spin-coating. The spin coater used was an Able Co. SP-1 spin programmer. The thickness of the dendrimer films was adjusted to 1 μm by a rotation speed of 800 rpm. The thickness was confirmed on a Tencor P-10 surface profiler after cutting a portion of

TABLE I
Calculated Molecular Weights (M), Weight-Average Molecular Weights (M_w), Number-Average Molecular Weights (M_n), and Polydispersity Indices (M_w/M_n) for the Dendrimers

	G2-PV-TPA	G3-PV-TPA
M	4229	8689
M_w[a] ($\times 10^3$)	4.5	7.7
M_n[a] ($\times 10^3$)	4.3	7.2
M_w/M_n	1.05	1.07

[a] Determined by GPC using THF as eluent.
Standard polystyrene samples were used for the calibration of the molecular weight.

the films. Next, a vacuum evaporator was used for the thermal evaporation of the alloy of 10 wt % Mg and 90 wt % Al (Mg–Al) onto the desired ITO glass plates deposited with dendrimer films.

Measurements

TOF measurements for the cells of ITO/dendrimer/Mg–Al were carried out with a conventional setup as described by Chen et al.[30] A pulsed N_2 laser (337.1 nm, pulse width 0.7 ns) having output of 150 μJ/pulse was used to generate photocarrier in the dendrimer films. The measurements were performed at 25°C in vacuum condition (10^{-3} Torr). The current generated as a result of photocarrier drift was collected across a 50 Ω resister upon application of an external bias voltage for periods of 250 μs. The charge-carrier drift mobility was determined by the following relation:

$$\mu = \frac{L^2}{T_{tr} V} \quad (1)$$

where μ is the charge-carrier drift mobility, L is the thickness of the dendrimer film, V is the applied bias voltage, and T_{tr} is the transit time derived from the double logarithmic plot of the photocurrent decay (Scher-Montroll plot).[31]

UV–vis absorption spectra were measured on a Shimadzu UV-3100PC spectrophotometer. The measurements were performed on 50 nm thick dendrimer films prepared by spin-coating with the rotation speed of 2500 rpm from 0.5 mg/mL chloroform solutions on glass substrates. Contribution from absorption of the glass substrate was corrected by subtracting from each absorption spectrum the glass substrate spectrum.

RESULTS AND DISCUSSION

Table I represents the calculated molecular weights (M), the weight and number average molecular weights (M_w, M_n) and the polydispersity indices (M_w/M_n) for the G2-PV-TPA and G3-PV-TPA dendrimers. For both dendrimers, the M_w/M_n values are close to 1, implying that the comparably monodispersed dendrimers are obtained. The difference between M and M_w or M_n for G2-PV-TPA is quite small, whereas the difference between M and M_w or M_n for G3-PV-TPA is comparably large. Since M_w and M_n are the converted molecular weights with the standard polystyrene, one can estimate that the difference would be large with increasing the molecular weight.

Before evaluation of charge-carrier transport property by the TOF technique, it is important to confirm the fact that the photocarrier generation takes place due to the irradiation of N_2 laser light. UV–vis absorption spectra for G2-PV-TPA and G3-PV-TPA dendrimer films with 50 nm thickness are shown in Figure 2. For both dendrimer films, two typical absorption peaks are observed centered at 300 and 370 nm, the former being due to the triphenylamine surface group, and the latter to the *p*-phenylenevinylene group.[27] It is obvious that the absorption bands for the triphenylamine and *p*-phenylenevinylene groups include the 337.1 nm wavelength of the N_2 laser light, confirming that the light absorption takes place by the N_2 laser irradiation.

By illuminating the N_2 laser light from the ITO side of the ITO/dendrimer/Mg–Al cells, photoexcited charge-carriers of hole and electron would generate at the surface of the dendrimer film. In case where a positive bias voltage is applied to the ITO side, the hole-carrier drifts from the ITO side to the Mg–Al side and photocurrent of positive sign will be observed. On the other hand, the electron-carrier drifts and photocurrent of negative sign will be observed as a negative bias voltage is applied to the ITO side. Photocurrent decays obtained from the ITO/G3-PV-TPA/Mg–Al cell are shown in Figure 3(a,b). Figure 3(a) indicates the photocurrent decay at applied bias voltage of +50 V, and Figure 3(b) the

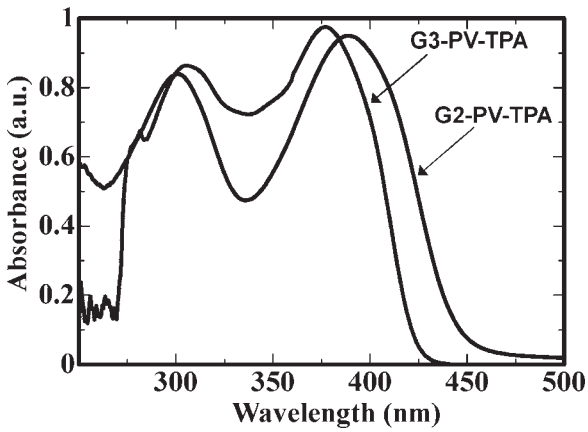

Figure 2 UV–vis absorption spectra for thin films of G2-PV-TPA and G3-PV-TPA.

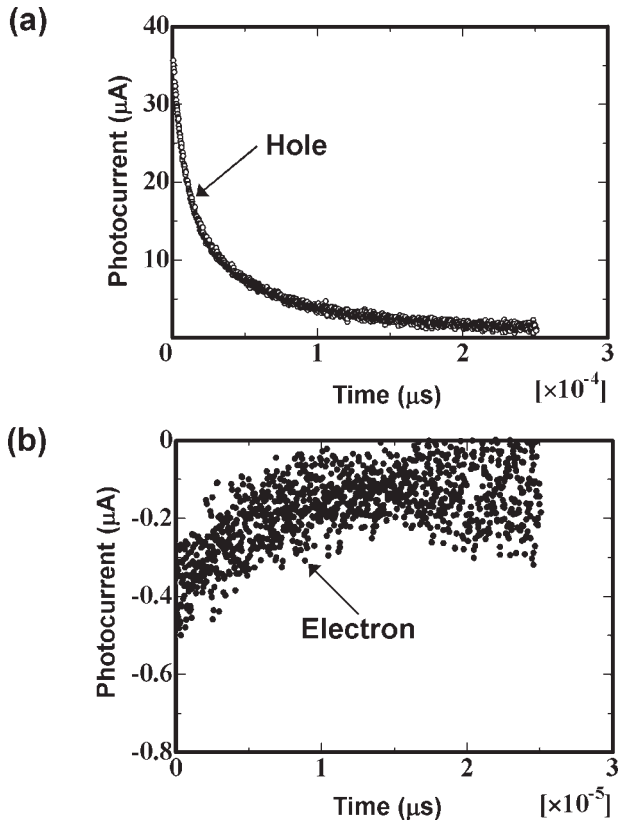

Figure 3 Profiles of photocurrent decays for the ITO/G3-PV-TPA/Mg–Al cell at applied bias voltage of (a) +50 V and (b) −50 V; (a) indicates hole-carrier transport and (b) indicates electron-carrier transport.

photocurrent decay at applied bias voltage of −50 V to the ITO side. Both Figure 3(a,b) show the photocurrents due to the drifts of hole- and electron-carrier, respectively. The fact implies that the photocarrier generation takes place at the surface of the dendrimer film by absorbing the N_2 laser light. When the positive bias voltage (+50 V) is applied to the ITO side, much larger photocurrent is observed compared with the case where the negative bias voltage (−50 V) is applied to the ITO side. This is the result that the hole-carrier transport takes place preferentially compared with the electron-carrier transport. It is well-known that both *p*-phenylenevinylene and triphenylamine moieties show typical hole-carrier transport properties.[7,11,14,24–27] Hence, the result is considered to be reasonable. Figure 4(a) shows the photocurrent decays of ITO/G3-PV-TPA/Mg–Al and ITO/G2-PV-TPA/Mg–Al cells at applied bias voltage of +25 V to the ITO side. The photocurrent for the ITO/G2-PV-TPA/Mg–Al cell is quite larger than that for the ITO/G3-PV-TPA/Mg–Al cell below 10 μs, implying that the efficiency of hole-carrier hopping in the G2-PV-TPA film is quite higher than that in the G3-PV-TPA film. The photocurrent decays for both dendrimer films shown in Figure 4(a) are typically dispersive, implying that the charge-carrier transport properties are typical conducting-polymer-film type.[11,25–28] As shown in this figure, dark current of each cell seems to be small enough to be negligible. Figure 4(b) shows the double logarithmic plots[31] (Scher-Montroll plots) of the photocurrent decays for both cells by applying +25 V to the ITO side, which are modified from Figure 4(a). The transit times (T_{tr}), which are the intercept of two tangential lines before and after the inflection point,[11,23–28,30,31] are observed for both cells. This is indicative that the hole-carriers travel across the dendrimer film and finally arrive to the Mg–Al side at T_{tr}. Though the inflection points are observed for both dendrimer films, the characteristics of the photocurrent decays are significantly different. In the case of the ITO/G2-PV-TPA/Mg–Al cell, the photocurrent value kept almost constant below the inflection point (about 3 μs), and the clear inflection point is observed at about 3 μs. On the other hand, the photocurrent value for the ITO/G3-PV-TPA/Mg–Al cell decreases even below the inflection point (i.e., 14 μs), and the unclear inflection point is observed at about 14 μs. One of the assumptions that the inflection point becomes unclear for the ITO/G3-PV-TPA/Mg–Al cell is that some amount of hole-carriers quench before arriving to

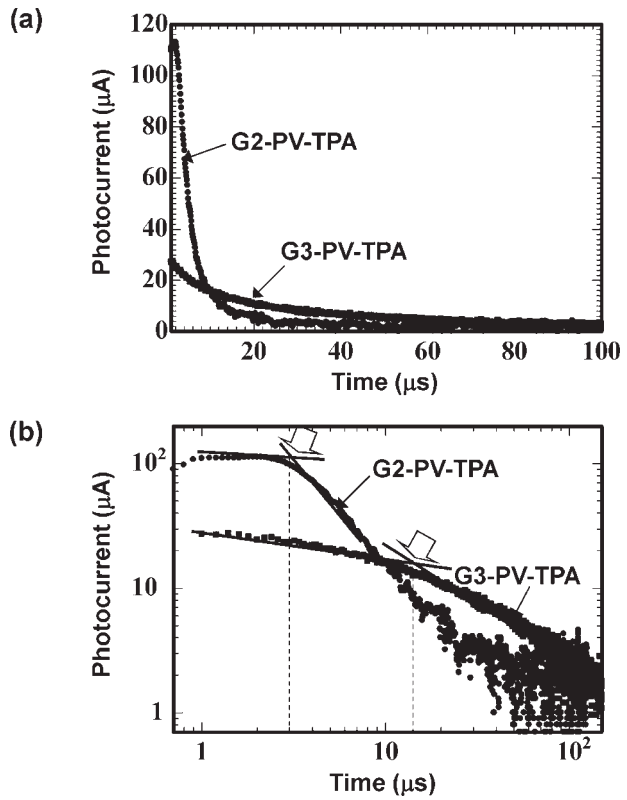

Figure 4 (a) Profiles of photocurrent decays for the ITO/G2-PV-TPA/Mg–Al and ITO/G3-PV-TPA/Mg–Al cells at applied bias voltage of +25 V, and (b) double logarithmic plots of the photocurrent decays (Scher-Montroll plots).

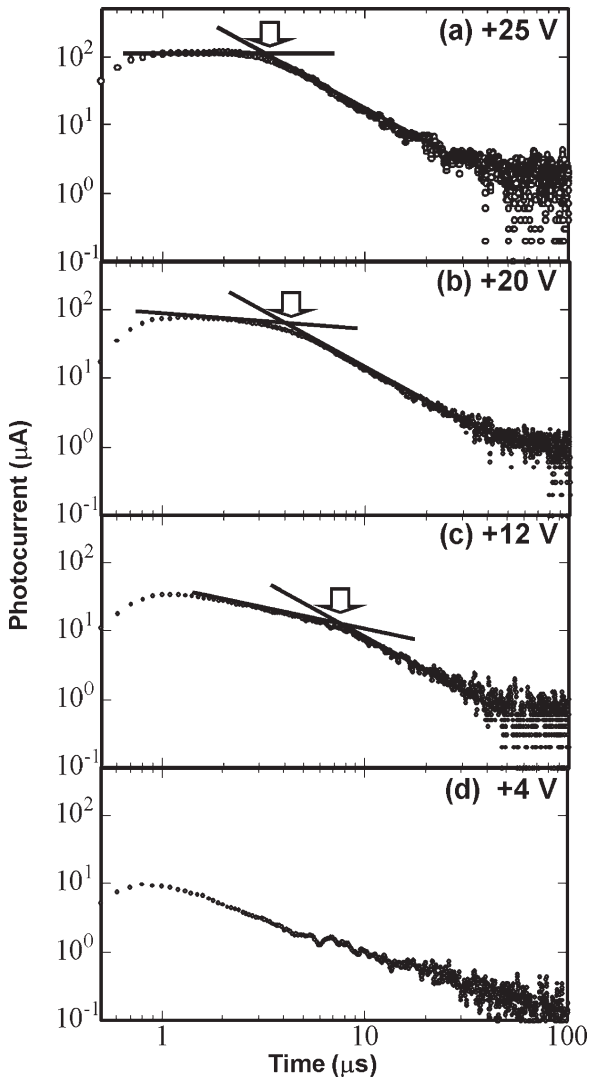

Figure 5 Double logarithmic plots of photocurrent decays (Scher-Montroll plots) for the ITO/G2-PV-TPA/Mg–Al cell at applied bias voltage of (a) +25 V, (b) +20 V, (c) +12 V, and (d) +4 V.

the Mg–Al electrode in the G3-PV-TPA film. The double logarithmic plots for the ITO/G2-PV-TPA/Mg–Al cell in the range of the applied bias voltage from +25 V to +4 V are presented in Figure 5(a–d). The inflection points are able to be observed in the range from + 25 V to + 12 V. The inflection point shifts to the longer time with decreasing applied bias voltage, being indicative that the hole-carrier transport velocity becomes small with decreasing applied bias voltage. Besides the result, it becomes difficult to distinguish the inflection point as the applied bias voltage becomes +4 V as shown in Figure 5(d). The fact that the inflection point becomes unobservable with decreasing applied bias voltage implies that some amount of the hole-carriers quench before arriving to the Mg–Al electrode since the hole-carrier transport velocity becomes significantly slow, which is the same tendency as the ITO/G3-PV-TPA/Mg–Al cell shown in Figure 4(b).

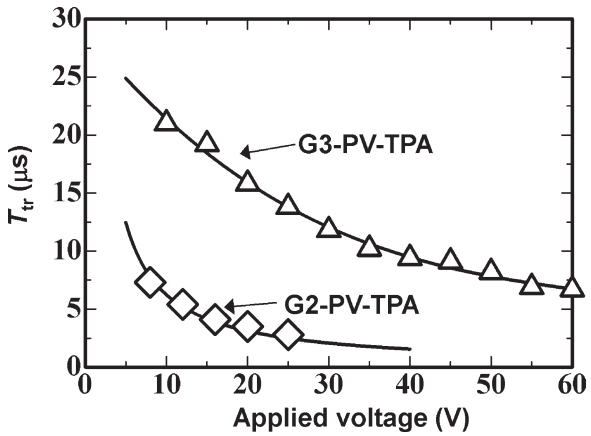

Figure 6 Inflection point (T_{tr}) as a function of applied bias voltage for G2-PV-TPA and G3-PV-TPA.

The values of the inflection points (T_{tr}) for both cells are plotted as a function of applied bias voltage in Figure 6. The T_{tr} values for both cells decrease with increasing applied bias voltage, indicating that the hole-carrier transport velocity becomes fast with increasing applied bias voltage. Also, the T_{tr} value for the ITO/G3-PV-TPA/Mg–Al cell is approximately three times larger than that for the ITO/G2-PV-TPA/Mg–Al cell at each bias voltage. The T_{tr} values for the ITO/G2-PV-TPA/Mg–Al cell are below 7.5 μs, whereas those for the ITO/G3-PV-TPA/Mg–Al cell reach to about 20 μs. This indicates that the hole-carrier transport velocity in the G2-PV-TPA film is faster than that in the G3-PV-TPA film.

Figure 7 represents the current values at T_{tr} (I_{tr}) for both cells as a function of applied bias voltage. I_{tr} for the ITO/G3-PV-TPA/Mg–Al cell increases linearly with increasing applied bias voltage. The increase in I_{tr} for the ITO/G3-PV-TPA/Mg–Al cell is considered to be due to increase in the hole-carrier

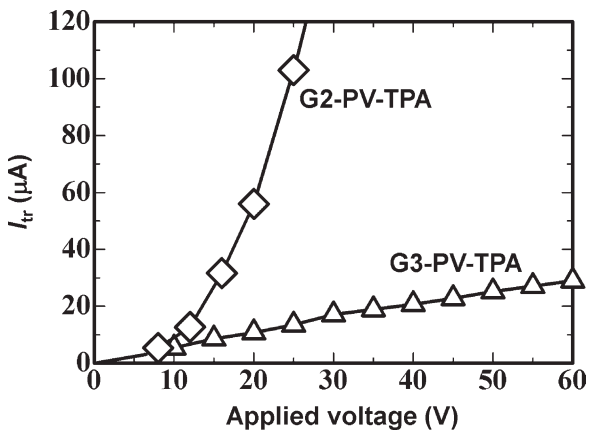

Figure 7 Photocurrent at T_{tr} (I_{tr}) as a function of applied bias voltage for G2-PV-TPA and G3-PV-TPA.

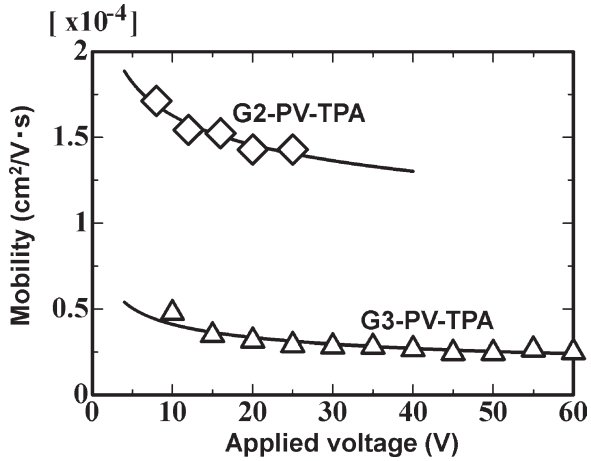

Figure 8 Hole-carrier drift mobility (μ) as a function of applied bias voltage for G2-PV-TPA and G3-PV-TPA.

transport velocity with increasing applied bias voltage. In contrast, I_{tr} for the ITO/G2-PV-TPA/Mg–Al cell increases with increasing applied bias voltage with a quadratic curve. The current value is considered to be represented by two factors, which are the transport velocity and the density of the charge-carrier shown in eq. (2).

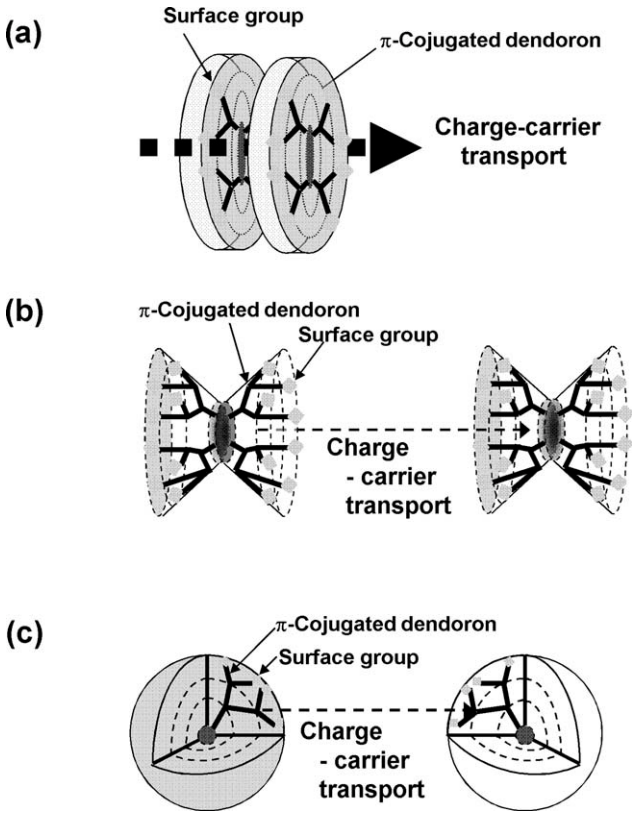

Figure 9 Schematic representations of charge-carrier transport systems for conducting dendrimers with molecular geometric structures of (a) planar-, (b) cylindrical-, and (c) globular-shape.

$$I \propto n\mu\frac{V}{L} \tag{2}$$

where I is the current value and n is the density of the transporting charge-carrier. In eq. (2), $\mu(V/L)$ is the transport velocity and is presumed to increase linearly with increasing applied bias voltage. Thus, the quadratic curve observed from the ITO/G2-PV-TPA/Mg–Al cell is due to increase not only in the hole-carrier transport velocity but also in the density of the hole-carrier arrived to the Mg–Al side with increasing applied bias voltage. The I_{tr} values for the ITO/G2-PV-TPA/Mg–Al cell are considerably larger than those for the ITO/G3-PV-TPA/Mg–Al cell. One can consider that there are two reasons of the result. One is that the hole-carrier drift mobility of the G2-PV-TPA film is larger than that of the G3-PV-TPA film, the other is that the density of the hole-carrier drifting across the G2-PV-TPA film is larger than that across the G3-PV-TPA film.

The hole-carrier drift mobilities, which are determined from eq. (1), for both cells as a function of applied bias voltage are depicted in Figure 8. The drift mobilities in the G2-PV-TPA film are approximately three times larger than those in the G3-PV-TPA film in the range of applied bias voltage from 12 V to 25 V. Particularly, the drift mobility of G2-PV-TPA reaches 1.7×10^{-4} cm^2/(V·s) at 25°C. This is indicative that the charge-carrier hopping takes place more efficiently in the G2-PV-TPA film rather than in the G3-PV-TPA film. One of the hypotheses for the difference of the drift mobility between G2-PV-TPA and G3-PV-TPA is due to the difference of the molecular geometric structure between the dendrimers. In case of a planar-shaped structure, the efficiency of charge-carrier hopping is presumed to be higher than those of globular- and cylindrical-shaped structures, because the mean distance between the planar-shaped molecules can be the smallest among the planar-, globular-, and cylindrical-shaped molecules in principle. Figure 9 illustrates the molecular geometric structures of the dendrimers and their charge-carrier transport systems. Meier et al.[32] reported that the molecular geometric structures of the first two generations for the *p*-phenylenevinylene dendrimers surrounded by the alkyloxy surface groups such as hexyloxy or dodecyloxy group exhibit the planar shapes. In

TABLE II
Diameter (D), Height (H), and D/H Ratios of the Dendrimers Obtained by MM3 Calculation Technique

	G2-PV-TPA	G3-PV-TPA
Diameter (D)/Å	46.7	56.5
Height (H)/Å	9.6	13.1
D/H	4.9	4.3

TABLE III
Molecular Weight Ratios of Nitrogen Atom and Triphenylamine to the Dendrimers

	G2-PV-TPA	G3-PV-TPA
M_N/M_D[a] ($\times 10^{-1}$)	6.9	6.7
M_{TPA}/M_D[b] ($\times 10^{-2}$)	4.0	3.9

[a] M_N indicates the calculated molecular weights of nitrogen atoms in the dendrimers. M_D indicates the calculated molecular weights of dendrimers, G2-PV-TPA and G3-PV-TPA.

[b] M_{TPA} indicates the calculated molecular weights of triphenylamine units in the dendrimers.

contrast to this, the higher generations are assumed to be the cylindrical shapes due to steric hindrance of the molecules.[32] The molecular geometric structures for the G2-PV-TPA and G3-PV-TPA dendrimers are evaluated by molecular mechanics program 3 (MM3) calculation technique as listed in Table II. The diameter (D) to height (H) ratio (D/H) for the G2-PV-TPA molecule is higher than that for the G3-PV-TPA molecule. This is indicative that the molecular geometric structure of G2-PV-TPA shows more planar than that of G3-PV-TPA. Thus, the larger hole-carrier drift mobilities for G2-PV-TPA are induced by higher degree of planar-shaped structure compared with G3-PV-TPA. Another possibility for the difference of the drift mobilities between G2-PV-TPA and G3-PV-TPA is the difference of the composition for the dendrimer molecule. There is a possibility that the nitrogen atom in the triphenylamine unit promotes the hole-carrier transport property, implying that the hole-carrier drift mobility would increase with increasing the molecular weight ratio of the nitrogen atom to the dendrimer molecule. Hence, the ratios for molecular weights of nitrogen atom (M_N) and triphenylamine unit (M_{TPA}) to the dendrimer molecule (M_D) are determined as shown in Table III. The M_N/M_D and M_{TPA}/M_D values for G2-PV-TPA are higher than those for G3-PV-TPA, indicating the possibility that the higher hole-carrier drift mobilities for G2-PV-TPA compared with those for G3-PV-TPA are due to the higher molecular weight ratio of nitrogen atom in the dendrimer.

It is to be noted that the hole-carrier drift mobilities for both dendrimer films decrease with increasing applied bias voltage as shown in Figure 8. Since the dark currents are enough small to be negligible, the negative electric field dependences are explained by disorder formalism as follows.[11,25,33] One can assume that the charge-carrier transport in disordered systems takes place by hopping through a manifold of localized states subject to the fluctuations of both hopping site energy and intermolecular wavefunction overlap and that both the hopping site energy and the intermolecular distance follow the Gaussian distributions. The disorder is known to be obtained for a variety of amorphous molecular glassy films.[11,25,33]

The hole-carrier drift mobilities of the dendrimers used in this work are on the orders of 10^{-5} and 10^{-4} ($cm^2/V{\cdot}s$) by the TOF technique. The hole-carrier drift mobility of poly(*p*-phenylenevinylene) is reported to be in the range of 10^{-5} ($cm^2/V{\cdot}s$) at 25°C,[24] indicating that the drift mobility of the poly(*p*-phenylenevinylene) is one order of magnitude smaller than that of G2-PV-TPA. Lee et al.[26] also reported that the hole-carrier drift mobilities of poly(*p*-phenylenevinylene)s having a series of fluorene side chains are in the range from 10^{-7} to 10^{-4} ($cm^2/V{\cdot}s$) at 25°C. The drift mobilities obtained for the dendrimers are included in this range. The comparisons between the dendrimers and several poly(*p*-phenylenevinylene)s indicate that the dendrimers are useful for the electronic and optoelectronic devices. The dendrimers used here also exhibit enough solubility to prepare the thin films with the solution processes. Hence, these are candidates for hole-carrier transporting materials toward large-sized OLEDs. In particular, the G2-PV-TPA dendrimer is a strong candidate because of the comparably large drift mobility.

CONCLUSIONS

Charge-carrier transport property of the conducting dendrimer films composed of *p*-phenylenevinylene with generation numbers of two and three as a dendron and triphenylamine as a surface group, G2-PV-TPA and G3-PV-TPA, prepared by spin-coating from the chloroform solutions was investigated by the TOF technique at 25°C. For both dendrimer films, hole-carrier transport took place preferentially compared with electron-carrier transport. Besides this, typical dispersive hole-carrier transport was observed for both dendrimer films. The hole-carrier drift mobilities of the G2-PV-TPA film were on the order of 10^{-4} ($cm^2/V{\cdot}s$), whereas those of the G3-PV-TPA film were on the order of 10^{-5} ($cm^2/V{\cdot}s$). The difference of the hole-carrier drift mobilities between G2-PV-TPA and G3-PV-TPA was due to the difference of the molecular geometric structure and/or the difference of the molecular weight ratio of nitrogen atom in the triphenylamine unit to the dendrimer molecule. The higher diameter to height ratio was obtained for the G2-PV-TPA molecule compared with G3-PV-TPA. Also, the higher molecular weight ratio of the nitrogen atom was obtained for G2-PV-TPA rather than G3-PV-TPA.

The results of the TOF study strongly indicate that the dendrimers used in this work are effective for hole-carrier transporting materials of large-sized OLEDs.

The author thank Toyo Gosei Co. for preparation of the conducting dendrimers.

References

1. Tang, C. W.; VanSlyke, S. A. Appl Phys Lett 1987, 51, 913.
2. Yoshino, K.; Kuwabara, T.; Iwasa, T.; Kawai, T.; Onoda, M. Jpn J Appl Phys 1990, 29, L1514.
3. Hoofman, R. J. O. M.; Haas, M.P. de; Siebbeles, L. D. A.; Warman, J. M. Nature 1998, 392, 54.
4. Morrison, J. J.; Murray, M. M.; Li, X. C.; Holmes, A. B.; Morratti, S. C.; Friend, R. H.; Sirringhaus, H. Synth Met 1999, 102, 987.
5. Dimitrakopoulos, C. D.; Malenfant, P. R. L. Adv Mater 2002, 14, 99.
6. Kaneto, K.; Hatae, K.; Nagamatsu, S.; Takashima, W.; Pandey, S. S.; Endo, K.; Rikukawa, M. Jpn J Appl Phys Part 2 1999, 38, L1188.
7. Martens, H. C. F.; Blom, P. W. M.; Schoo, H. F. M. Phys Rev B 2000, 61, 7489.
8. Cravino, A.; Roquet, S.; Aleveque, O.; Leriche, P.; Frere, P.; Roncali, J. Chem Mater 2006, 18, 2584.
9. Li, Y.; Wu, Y.; Liu, P.; Birau, M.; Pan, H.; Ong, B. S. Adv Mater 2006, 18, 3029.
10. Wang, Y.; Zhou, E.; Liu, Y.; Xi, H.; Ye, S.; Wu, W.; Guo, Y.; Di, C.-A.; Sun, Y; Yu, G; Li, Y. Chem Mater 2007, 19, 3361.
11. Shirota, Y.; Kageyama, H. Chem Rev 2007, 107, 953.
12. Shirota, Y.; Kobata, T.; Noma, N. Chem Lett 1989, 18, 1145.
13. Higuchi, A.; Inada, H.; Kobata, T.; Shirota, Y. Adv Mater 1991, 3, 549.
14. Shirota, Y.; Kuwabara, Y.; Inada, H.; Wakimoto, T.; Nakada, H.; Yonemoto, Y.; Kawami, S.; Imai, K. Appl Phys Lett 1994, 65, 807.
15. Ishikawa, W.; Inada, H.; Nakano, H.; Shirota, Y. Chem Lett 1991, 20, 1731.
16. Ishikawa, W.; Inada, H.; Nakano, H.; Shirota, Y. Mol Cryst Liq Cryst 1992, 211, 431.
17. Inada, H.; Shirota, Y. J Mater Chem 1993, 3, 319.
18. Bettignies, R. de; Nicolas, Y.; Blanchard, P.; Levillain, E.; Nunzi, J.-M.; Roncali, J. Adv Mater 2003, 15 1939.
19. Roquet, S.; Cravino, A.; Leriche, P.; Aleveque, O.; Frere, P.; Roncali, J. J Am Chem Soc 2006, 128, 3459.
20. Cravino, A.; Leriche, P.; Aleveque, O.; Roquet, S.; Roncali, J. Adv Mater 2006, 18, 3033.
21. Horowitz, G. Adv Mater 1998, 10, 365.
22. Katz, H. E. J Mater Chem 1997, 7, 369.
23. Pandey, S. S.; Nagamatsu, S.; Takashima, W.; Kaneto, K. Jpn J Appl Phys Part 1 2000, 39, 6309.
24. Lededev, E.; Dittrich, Th.; Petrova-Koch, V.; Karg, S.; Brutting, W. Appl Phys Lett 1997, 71, 2686.
25. Hertel, D.; Bassler, H.; Scherf, U.; Horhold, H. H. J Chem Phys 1999, 110, 9214.
26. Lee, S. H.; Yasuda, T.; Tsutsui, T. J Appl Phys 2004, 95, 3825.
27. Lupton, J. M.; Samuel, I. D. W.; Beavington, R.; Burn, P. L.; Bassler, H. Synth Met 2001, 116, 357.
28. Markham, J. P. J.; Samuel, I. D. W.; Lo, S.-C.; Burn, P. L.; Weiter, M.; Bassler, H. J Appl Phys 2004, 95, 438.
29. Yamahara, M.; Obara, S.; Tada, K. Jpn Pat 2004, 18539.
30. Chen, B.; Lee, C.-S.; Lee, S.-T.; Webb, P.; Chan, Y.-C.; Gambling, W.; Tian, H.; Zhu, W. Jpn J Appl Phys Part 2 2000, 39, 1190.
31. Scher, H.; Montroll, E. W. Phys Rev B 1975, 12, 2455.
32. Meier, H.; Lehmann, M.; Kolb, U. Chem Eur J 2000, 6, 2462.
33. Bassler, H. Phys Status Solidi B 1993, 175, 15.